

# A Discontinuous Galerkin Consistent Splitting Method for the Incompressible Navier–Stokes Equations

Dominik T. Still <sup>\*‡</sup>    Natalia Nebulishvili <sup>†‡</sup>    Richard Schussnig <sup>†</sup>  
 Katharina Kormann <sup>†</sup>    Martin Kronbichler <sup>†</sup>

December 8, 2025

## Abstract

This work presents the discontinuous Galerkin discretization of the consistent splitting scheme proposed by Liu [J. Liu, J. Comp. Phys., 228(19), 2009]. The method enforces the divergence-free constraint implicitly, removing velocity–pressure compatibility conditions and eliminating pressure boundary layers. Consistent boundary conditions are imposed, also for settings with open and traction boundaries. Hence, accuracy in time is no longer limited by a splitting error.

The symmetric interior penalty Galerkin method is used for second spatial derivatives. The convective term is treated in a semi-implicit manner, which relaxes the CFL restriction of explicit schemes while avoiding the need to solve nonlinear systems required by fully implicit formulations. For improved mass conservation, Leray projection is combined with divergence and normal continuity penalty terms.

By selecting appropriate fluxes for both the divergence of the velocity field and the divergence of the convective operator, the consistent pressure boundary condition can be shown to reduce to contributions arising solely from the acceleration and the viscous term for the  $L^2$  discretization.

Per time step, the decoupled nature of the scheme with respect to the velocity and pressure fields leads to a single pressure Poisson equation followed by a single vector-valued convection-diffusion-reaction equation. We verify optimal convergence rates of the method in both space and time and demonstrate compatibility with higher-order time integration schemes. A series of numerical experiments, including the two-dimensional flow around a cylinder benchmark and the three-dimensional Taylor–Green vortex problem, verify the applicability to practically relevant flow problems.

**Keywords.** time-splitting methods, consistent splitting, discontinuous Galerkin, fractional-step scheme, IMEX, incompressible Navier–Stokes

## 1 Introduction

Incompressible fluid flows play a major role in science and engineering, including countless applications of immense societal value. Computational fluid dynamics aims to provide approximate solutions with the help of computer simulation and has become a fundamental discipline, immediately transferring to other areas of research and technology. Great progress has been made over the past decades, but even the high-performance implementations of high-fidelity algorithms available today continue to challenge today’s largest compute clusters. In a decades-long endeavor, accuracy and throughput of related numerical algorithms and their implementation have been continuously improved. However, further advancements are still urgently needed due to increasing demand in terms of accuracy, time to solution, numerical robustness, or conservation properties and physics conformity. The innovations are often driven by challenging high-resolution applications in the energy, aviation or combustion sectors, or motivated by the

<sup>\*</sup>Institute for Computational Mechanics, TUM School of Engineering and Design, Technical University of Munich (dominik.still@tum.de).

<sup>†</sup>Ruhr University Bochum - Faculty of Mathematics (natalia.nebulishvili@rub.de, richard.schussnig@rub.de, k.kormann@rub.de, martin.kronbichler@rub.de).

<sup>‡</sup>These authors contributed equally to this work.

requirements of many-query applications such as uncertainty quantification, sensitivity analysis, model order reduction, inverse problem analysis and machine learning.

The Navier–Stokes equations for incompressible flows are typically integrated via implicit time integrators due to the divergence-free or incompressibility constraint. Via the divergence-free condition, the pressure acts as a Lagrange multiplier enforcing the continuity of mass. This structure calls for specific choices of spaces for velocity and pressure approximation to fulfill the so-called inf-sup (Ladyzhenskaya–Babuška–Brezzi) condition [1, 2]. Since the ground-breaking work by Hood and Taylor [3], who first used inf-sup stable velocity–pressure pairs, the finite element method has been established as a viable alternative to the finite volume method. For inf-sup stability and suitable stabilization, see for instance [4–7].

The standard time discretization approach, considering the mixed problem governing velocity and pressure fields as a large differential-algebraic system, leads to linear systems of saddle-point structure. Depending on the flow regime and problem parameters, the pressure Schur complement can be approximated by pressure mass and Poisson operators [8], while convective-dominant settings can be tackled via, e.g., augmented-Lagrangian-based approaches [9–12]. However, these approaches can lead to an ill-conditioned velocity-velocity block, which in turn necessitates specialized multigrid methods, see, e.g., [13].

Other—typically less Reynolds-robust alternatives—are the pressure convection-diffusion [14, 15] and least-squares commutator [16, 17] preconditioners, which can perform well, especially for reasonable time step size and grid quality. Some of these concepts have also been extended towards more complex physics, in the simplest case captured by nonlinear viscosity, used in, e.g., earth mantle convection [18], multiphase flows [19], or generalized Newtonian fluids [7]. Recent research has tried to re-formulate the partial differential equations underlying the saddle-point problem to simplify the linear algebra aspects [20].

To (seemingly) avoid the compatibility conditions between velocity and pressure spaces for the finite element method, a class of schemes, the so-called splitting, projection, or fractional-step schemes, circumvent solving a monolithic system at each time step by decoupling the governing equations for the velocity and pressure. This also simplifies the design of preconditioners, at the expense of more complex boundary conditions for the Poisson problem governing the pressure. Relevant examples are incremental pressure-correction methods in rotational form as described in [21, 22], the dual splitting scheme by Karniadakis et al. [23], see also [24], the consistent splitting schemes by Guermond and Shen [25] and Liu [26] (see also the related method developed by Huang and Shen [27]). Recent developments in this regard focus among other directions on the non-trivial extensions towards complex rheological laws [28–30], unconditional stability beyond second-order accurate schemes following ideas by Huang and Shen [27], as well as multiphase flows [31, 32] and fluid–structure interaction [33].

In this context, the present article focuses on spatial discretizations of higher-order accurate discontinuous Galerkin (DG) discretizations of the consistent splitting scheme by Liu [26] and thorough testing of the resulting framework. The motivation for choosing the consistent splitting over classical projection schemes is to avoid pressure boundary layers and achieve higher-order accuracy in time, while avoiding solving the monolithic system arising in mixed formulations. In contrast to the approach of Liu [26], which employs continuous finite elements, the DG discretization offers high-order accuracy combined with improved robustness in convection-dominated regimes [34]. The closest competitors are shortly commented on in what follows.

First, compared to the dual splitting scheme by Karniadakis et al. [23] and its robust DG discretization presented by Fehn et al. [35, 36], the present scheme employs consistent boundary conditions for the pressure Poisson equation and enables equal-order  $C^0$ -continuous interpolation [6, 37] according to numerical evidence. Furthermore, it is an important step towards unconditional stability for higher-order timestepping schemes, as the method can be extended adopting ideas by Huang and Shen [27]. Second, Rosales et al. [38] adopted the consistent splitting scheme and employed higher-order implicit-explicit Runge–Kutta schemes. However, they introduced the vorticity  $\omega = \nabla \times \mathbf{u}$  as an additional unknown to enforce the so-called electric boundary conditions naturally, a complication we can avoid due to the fact that we want to enforce a different set of boundary conditions, as will be discussed shortly. Third, Li et al. [39] present a higher-order method based on the consistent splitting idea for the variable-density Navier–Stokes equations. They employ a DG method with bound-preserving limiter for the density evolution and continuous Galerkin schemes for the pressure and momentum equations combined with fully explicit and implicit-explicit Runge–Kutta timesteppers. Compared to their work, we do not consider variable viscosity, but aim to improve robustness with respect to convective effects via DG discretization of the momentum equation.

The paper is organized as follows: Sec. 2 presents the fundamental idea behind consistent splitting

schemes, leading to the temporal discretization presented in Sec. 3. The  $L^2$ -conforming DG discretization is discussed in Sec. 4. The properties of the devised numerical methods are critically investigated in Sec. 5, including spatial and temporal convergence studies in Sec. 5.1 on exact solutions, and the practically relevant benchmarks of flow around a cylinder [40], see Sec. 5.2, and the 3D Taylor–Green vortex problem [41, 42], see Sec. 5.3. Concluding remarks are given in Sec. 6.

## 2 Consistent Splitting Scheme

### 2.1 The Navier–Stokes Equations for Incompressible Flows

We consider the Navier–Stokes equations governing the incompressible flow of a viscous fluid within the spatial domain  $\Omega \subset \mathbb{R}^d$  with  $d = 2$  or  $3$ . They consist of the momentum balance equation

$$\frac{\partial \mathbf{u}}{\partial t} + (\mathbf{u} \cdot \nabla) \mathbf{u} - \nu \Delta \mathbf{u} + \nabla p = \mathbf{f} \quad \text{in } \Omega \times [0, T], \quad (1)$$

where  $\nu$  is the kinematic viscosity, and the continuity equation

$$\nabla \cdot \mathbf{u} = 0 \quad \text{in } \Omega \times [0, T]. \quad (2)$$

The system is initialized with a divergence-free initial condition

$$\mathbf{u}(\mathbf{x}, t = 0) = \mathbf{u}_0(\mathbf{x}) \quad \text{in } \Omega. \quad (3)$$

The boundary  $\Gamma = \partial\Omega$  is split into non-overlapping Dirichlet and Neumann boundaries, denoted by  $\Gamma^D$  and  $\Gamma^N$ , respectively, such that  $\Gamma = \Gamma^D \cup \Gamma^N$  and  $\Gamma^D \cap \Gamma^N = \emptyset$ . On the Dirichlet and Neumann boundary segments the following conditions hold

$$\mathbf{u} = \mathbf{g} \quad \text{on } \Gamma^D \times [0, T], \quad (4)$$

$$(\nu \nabla \mathbf{u} - p \mathbb{I}) \mathbf{n} = \mathbf{h} \quad \text{on } \Gamma^N \times [0, T]. \quad (5)$$

Here,  $\mathbf{n}$  denotes the unit outward normal vector.

### 2.2 Consistent Splitting

Standard implicit discretization of the Navier–Stokes problem (1)–(5) adopting a mixed finite element method leads to a nonlinear system in saddle-point form. An attractive alternative is found in consistent splitting schemes, which split the coupled velocity-pressure system, resulting in a Poisson problem for the pressure and a convection-diffusion problem for the momentum equation. As proposed by Liu [26], the consistent splitting method replaces the incompressibility constraint by a pressure Poisson equation (PPE)

$$-\Delta p = \nabla \cdot (\mathbf{u} \cdot \nabla \mathbf{u}) - \nabla \cdot \mathbf{f} \quad \text{in } \Omega \times [0, T], \quad (6)$$

by taking the divergence of Eq. (1) and using the divergence of the time derivative and the viscous term being zero under suitable regularity assumptions. To obtain a boundary condition for the PPE on the Dirichlet portion  $\Gamma_D$ , Eq. (1) is dotted with the normal vector  $\mathbf{n}$  to obtain

$$\nabla p \cdot \mathbf{n} = \left[ -\frac{\partial \mathbf{g}}{\partial t} - (\mathbf{u} \cdot \nabla) \mathbf{u} + \mathbf{f} \right] \cdot \mathbf{n} - \nu \nabla \times (\nabla \times \mathbf{u}) \cdot \mathbf{n} \quad \text{on } \Gamma_D. \quad (7)$$

Here, we use the vector identity  $\Delta \mathbf{u} \equiv \nabla(\nabla \cdot \mathbf{u}) - \nabla \times (\nabla \times \mathbf{u})$  to realize the viscous term in curl form as advantageous for splitting methods [43]. The Neumann boundary data is further split into a viscous part  $\mathbf{h}_u$  and a pressure part  $g_p$  to obtain the Neumann boundary condition for the PPE as follows

$$\mathbf{h} \equiv \mathbf{h}_u - g_p \mathbf{n}, \quad (8)$$

with

$$\mathbf{h}_u := \nu (\nabla \mathbf{u}) \mathbf{n} \quad \text{on } \Gamma^N \times [0, T], \quad (9)$$

$$g_p := p \quad \text{on } \Gamma^N \times [0, T]. \quad (10)$$

It allows to apply the Neumann boundary data directly in the momentum equation and the PPE. Note that this choice also aligns with the most practically relevant scenarios, as frequently the pressure value is to be prescribed on open boundaries such as outflow. This boundary condition could also be based on an extrapolation of the viscous term in time, avoiding the split introduced in Eqs. (9)–(10). Such considerations are beyond the scope of the present work and are hence not considered in the following. For a detailed discussion on this topic for this splitting scheme see [44].

### 3 Discretization in Time

Within this work, backward differentiation formulae (BDF) are applied for time integration. The time interval of interest  $(0, T]$  is decomposed into time steps of size  $\Delta t$  from  $t^n$  to  $t^{n+1}$ . The scheme is written in the pressure-approximation form of [45], while the presentation of the individual steps is chosen similarly to [29]. Liu et al. [45] showed that the method achieves the convergence order  $\mathcal{O}(\Delta t^J)$  for a BDF scheme of order  $J$ . The pressure Poisson equation is solved first with extrapolated velocity terms on the right-hand side based on data from previous time steps, after which the momentum equation is used to compute the velocity.

#### Pressure Step

For the time derivative of the velocity in the momentum equation, a BDF scheme of order  $J$  is selected. An extrapolation of order  $J_c$  is employed for the convective term on the right-hand side of the PPE with  $J_c = J$  or  $J_c = J - 1$  to enhance numerical stability—especially in the higher-order case.

To compute the pressure at a new time step, denoted by  $p^{n+1}$ , the PPE is solved via

$$-\Delta p^{n+1} = \sum_{i=1}^{J_c} \bar{\beta}_i \nabla \cdot [(\mathbf{u}^{n+1-i} \cdot \nabla) \mathbf{u}^{n+1-i}] - \nabla \cdot \mathbf{f}^{n+1}. \quad (11)$$

with suitable extrapolation coefficients  $\bar{\beta}_i$ ,  $i = 1, \dots, J_c$  (see, e.g., Hairer et al. [46]). In the consistent boundary condition, the convective term is again extrapolated with order  $J_c$ , while for the viscous term an extrapolation order  $J_p$  can be chosen independently. Again suitable candidates are  $J_p = J$  or  $J_p = J - 1$ . The PPE is then subject to the boundary condition

$$\begin{aligned} \nabla p^{n+1} \cdot \mathbf{n} &= \sum_{i=1}^{J_c} \bar{\beta}_i [- (\mathbf{g}^{n+1-i} \cdot \nabla) \mathbf{u}^{n+1-i}] + \sum_{i=1}^{J_p} \hat{\beta}_i [-\nu \nabla \times (\nabla \times \mathbf{u}^{n+1-i})] \cdot \mathbf{n} \\ &- \partial_t \mathbf{g}^{n+1} \cdot \mathbf{n} + \mathbf{f}^{n+1} \cdot \mathbf{n} \quad \text{on } \Gamma_D, \end{aligned} \quad (12)$$

with appropriate coefficients  $\hat{\beta}_i$  for  $J_p$ . The effects of choosing different orders for  $J$ ,  $J_c$  and  $J_p$  are later shown for a numerical example in Tab. 5. On  $\Gamma_N$ , we can directly apply the decomposition  $p = g_p$  from Eq. (10). Alternatively, one might use the full traction condition given in Eq. (5), and incorporate the known extrapolated velocity in the viscous stress contribution. If the time derivative of the boundary condition  $\partial_t \mathbf{g}^{n+1}$  is not known analytically, a BDF scheme of order  $J$  is employed for approximation [35].

#### Momentum Step

With the known pressure  $p^{n+1}$ , the velocity  $\mathbf{u}^{n+1}$  at time  $t^{n+1}$  is computed by solving

$$\frac{\gamma_0}{\Delta t} \mathbf{u}^{n+1} + (\mathbf{u}^* \cdot \nabla) \mathbf{u}^{n+1} - \nu \nabla \cdot (\nabla \mathbf{u}^{n+1}) = \mathbf{f}^{n+1} + \sum_{i=1}^J \frac{\alpha_i}{\Delta t} \mathbf{u}^{n+1-i} - \nabla p^{n+1}, \quad (13)$$

where  $\gamma_0$  and  $\alpha_i$ ,  $i = 1, \dots, J$ , are suitable time integration constants (see, e.g., Hairer et al. [46]), and  $\mathbf{u}^* := \sum_{i=1}^J \beta_i \mathbf{u}^{n+1-i}$  is the extrapolated velocity linearizing the convective term. The convective term, written in semi-implicit formulation, relaxes the strict CFL conditions given by treating convection fully explicitly, while also avoiding the need to solve a nonlinear system of equations as resulting from fully implicit time integration, yet all options produce valid schemes, see also [29] and [47] for more general discussions on implicit-explicit schemes.

### 3.1 Leray Projection

The divergence-free condition is only implicitly enforced when adopting the consistent splitting scheme by Liu [26], which is rooted in the PPE replacing the continuity equation to begin with. To additionally suppress the divergence in the velocity field, we employ a Helmholtz–Leray decomposition,

$$\mathbf{u} = \hat{\mathbf{u}} - \nabla\phi, \quad (14)$$

see Liu [26], Pacheco et al. [29] for a more detailed discussion. In this presentation,  $\hat{\mathbf{u}}$  is solenoidal (divergence-free at every point), while  $\nabla\phi$  is irrotational. This splitting can be used to derive the so-called Leray projection by taking the divergence of Eq. (14)

$$\begin{aligned} \nabla \cdot \mathbf{u} &= \nabla \cdot \hat{\mathbf{u}} - \nabla \cdot \nabla\phi \\ \Leftrightarrow \nabla \cdot \mathbf{u} &= -\nabla \cdot \nabla\phi. \end{aligned} \quad (15)$$

Eq. (15) is completed with homogeneous Dirichlet and Neumann boundary conditions

$$\mathbf{n} \cdot \nabla\phi = 0 \quad \text{on } \Gamma_D, \quad \text{and} \quad \phi = 0 \quad \text{on } \Gamma_N. \quad (16)$$

The velocity  $\hat{\mathbf{u}} = \mathbf{u} + \nabla\phi$  is then completely divergence-free. Note, however, that  $\hat{\mathbf{u}}$  does not fulfill the tangential boundary conditions of the original problem. This can easily be shown by forming the dot product of the Helmholtz–Leray decomposition (14) with a tangential unit vector  $\boldsymbol{\tau}$  which yields

$$\boldsymbol{\tau} \cdot \hat{\mathbf{u}} = \boldsymbol{\tau} \cdot \mathbf{u} + \boldsymbol{\tau} \cdot \nabla\phi.$$

Simultaneously, we obtain the correct normal boundary condition of  $\mathbf{u}$

$$\mathbf{n} \cdot \hat{\mathbf{u}} = \mathbf{n} \cdot \mathbf{u} + \mathbf{n} \cdot \nabla\phi = \mathbf{n} \cdot \mathbf{u}$$

due to the boundary condition for the normal derivative of  $\phi$  on  $\Gamma_D$ , see Eq. (16). This dilemma forces us to choose between a) a not strictly divergence-free velocity field with correct boundary conditions obtained via the standard form we started with given in Eqs. (11)–(13), or b) a solenoidal velocity field  $\hat{\mathbf{u}}$  which does not fulfill the tangential boundary conditions as desired.

Following Liu [26], Pacheco et al. [29] among others, we apply the Leray projection only for the velocities of old time steps.

According to Liu [26] the divergence-free velocity field  $\hat{\mathbf{u}}$  is employed in the acceleration term on the right-hand side of Eq. (13), such that the right-hand side can be rewritten as

$$\begin{aligned} \mathbf{f}^{n+1} + \sum_{i=1}^J \frac{\alpha_i}{\Delta t} \hat{\mathbf{u}}^{n+1-i} - \nabla p^{n+1} &= \mathbf{f}^{n+1} + \sum_{i=1}^J \frac{\alpha_i}{\Delta t} (\mathbf{u}^{n+1-i} + \nabla\phi^{n+1-i}) - \nabla p^{n+1} \\ &= \mathbf{f}^{n+1} + \sum_{i=1}^J \frac{\alpha_i}{\Delta t} \mathbf{u}^{n+1-i} - \nabla \hat{p}^{n+1}, \end{aligned} \quad (17)$$

with the Leray projection applied at the old time steps. Instead of computing  $\phi$  explicitly, a modified pressure  $\hat{p}^{n+1} := p^{n+1} - \sum_{i=1}^J \alpha_i/\Delta t \phi^{n+1-i}$  is defined, which appears on the right-hand side of the momentum equation. This approach eliminates the computational overhead otherwise introduced by Eq. (15). The modified PPE can then be formulated as

$$\begin{aligned} -\Delta \hat{p}^{n+1} &= -\Delta p^{n+1} + \sum_{i=1}^J \frac{\alpha_i}{\Delta t} \Delta\phi^{n+1-i} \\ &= \sum_{i=1}^{J_c} \bar{\beta}_i \nabla \cdot [(\mathbf{u}^{n+1-i} \cdot \nabla) \mathbf{u}^{n+1-i}] - \nabla \cdot \mathbf{f}^{n+1} - \sum_{i=1}^J \frac{\alpha_i}{\Delta t} \nabla \cdot \mathbf{u}^{n+1-i}. \end{aligned} \quad (18)$$

Altogether, to solve the momentum step, the pressure  $p^{n+1}$  is substituted by  $\hat{p}^{n+1}$  in Eq. (13), and the PPE is substituted by the modified PPE (18). Note that due to the boundary conditions of  $\phi$  given in Eq. (16), Eq. (12) is not affected and remains unaltered. Comparing the present approach to [45], one observes that the convective term in the modified PPE and the boundary condition is treated with order  $J_c$  instead of  $J$ , giving more flexibility.

## 4 Discretization in Space

In this section the discretization with a  $L^2$ -conforming discontinuous Galerkin method is described. To this end, the spatial domain  $\Omega$  is approximated by  $N_{\text{el}}$  non-overlapping elements  $\Omega_e$ ,  $e = 1, \dots, N_{\text{el}}$ , such that  $\Omega \approx \Omega_h := \bigcup_{e=1}^{N_{\text{el}}} \Omega_e$ . The spaces of the test and ansatz functions are defined as

$$\begin{aligned} \mathcal{V}_h^u &= \left\{ \mathbf{u}_h \in [L^2(\Omega_h)]^d : \mathbf{u}_h(\mathbf{x}(\boldsymbol{\xi}))|_{\Omega_e} = \tilde{\mathbf{u}}_h^e(\boldsymbol{\xi})|_{\tilde{\Omega}_e} \in V_{h,e}^u = [\mathbb{P}_{k_u}(\tilde{\Omega}_e)]^d, \forall e = 1, \dots, N_{\text{el}} \right\}, \\ \mathcal{V}_h^p &= \left\{ p_h \in L^2(\Omega_h) : p_h(\mathbf{x}(\boldsymbol{\xi}))|_{\Omega_e} = \tilde{p}_h^e(\boldsymbol{\xi})|_{\tilde{\Omega}_e} \in V_{h,e}^p = \mathbb{P}_{k_p}(\tilde{\Omega}_e), \forall e = 1, \dots, N_{\text{el}} \right\}, \end{aligned} \quad (19)$$

where  $\mathbf{x}$  is the spatial coordinate in one of the elements  $\Omega_e$ , connected to the reference element  $\tilde{\Omega}_e$  with reference coordinate  $\boldsymbol{\xi}$  via an element-wise isoparametric mapping. On the reference element, the polynomial space  $\mathbb{P}_k$  of degree  $k$  is constructed via Lagrange polynomials. Within this work, inf-sup stable velocity-pressure pairings are considered, i.e.,  $k_u = k_p + 1$ . The functions  $\mathbf{u}_h \in \mathcal{V}_h^u$  and  $p_h \in \mathcal{V}_h^p$  approximate the velocity and the pressure, while the test functions from the velocity and pressure space are denoted by  $\mathbf{v}_h \in \mathcal{V}_h^u$  and  $q_h \in \mathcal{V}_h^p$ , respectively. Note, however, that for simplicity of notation, the discrete test and trial functions (unless stated otherwise) are written as  $\mathbf{u}$ ,  $\mathbf{v}$ ,  $p$  and  $q$ . We further define the jump and average operators along inner faces as

$$[[(\cdot)]] := (\cdot)_- - (\cdot)_+ \quad \text{and} \quad \{ \{ (\cdot) \} \} := 1/2 ((\cdot)_- + (\cdot)_+),$$

where  $(\cdot)$  might be scalar or vector-valued. Here,  $(\cdot)_-$  denotes quantities on the current element, while  $(\cdot)_+$  denotes quantities on the neighboring element. At the boundary, we adopt the mirror principle following Hesthaven and Warburton [34] wherever applicable to define an outer state  $(\cdot)_+$  that enforces boundary conditions weakly.

### 4.1 Pressure Poisson Step

The symmetric interior penalty Galerkin (SIPG) discretization [48–50] is chosen for the PPE (18) to avoid introducing auxiliary variables. The primal formulation reads: Find  $\hat{p}^{n+1} \in \mathcal{V}_h^p$  such that

$$l_p(\hat{p}^{n+1}, q) = r_p(\mathbf{u}_{i=1, \dots, J}^{n+1-i}, \mathbf{f}^{n+1}, \mathbf{g}_{i=1, \dots, J}^{n+1-i}, q), \quad (20)$$

for all  $q \in \mathcal{V}_h^p$  and all elements  $\Omega_e \in \Omega_h$ . Here, the left-hand side  $l_p$  is defined as

$$\begin{aligned} l_p(\hat{p}^{n+1}, q) &:= (\nabla \hat{p}^{n+1}, \nabla q)_{\Omega_e} \\ &\quad - \left( \nabla q, \frac{1}{2} [[\hat{p}^{n+1}]] \mathbf{n} \right)_{\partial \Omega_e \setminus \Gamma_h} - (\nabla q, \hat{p}_-^{n+1} \mathbf{n})_{\partial \Omega_e \cap \Gamma_N} \\ &\quad - (q, \{ \{ \nabla \hat{p}^{n+1} \} \} \cdot \mathbf{n})_{\partial \Omega_e \setminus \Gamma_h} - (q, \nabla \hat{p}_-^{n+1} \cdot \mathbf{n})_{\partial \Omega_e \cap \Gamma_N} \\ &\quad + (q, \tau [[\hat{p}^{n+1}]])_{\partial \Omega_e \setminus \Gamma_h} + (q, 2\tau \hat{p}_-^{n+1})_{\partial \Omega_e \cap \Gamma_N}, \end{aligned} \quad (21)$$

with the stabilization parameter  $\tau$  chosen according to Hillewaert [51].

The right-hand side  $r_p$  consists of the contributions from the body force  $\mathbf{f}$ , the terms stemming from the convective operator, the time derivative, the viscous term, the Leray projection and the inhomogeneous part of the SIPG discretization.

$$\begin{aligned} r_p(\mathbf{u}_{i=1, \dots, J}^{n+1-i}, \mathbf{f}^{n+1}, \mathbf{g}_{i=1, \dots, J}^{n+1-i}, q) &:= r_f(\mathbf{f}^{n+1}, q) + \sum_{i=1}^{J_c} \bar{\beta}_i r_{\text{conv}}(\mathbf{u}^{n+1-i}, \mathbf{g}^{n+1-i}, q) \\ &\quad + r_{\text{SIPG}}(g_p^{n+1}, \mathbf{u}^{n+1-i}, \mathbf{g}^{n+1}, q) - \sum_{i=1}^J \frac{\alpha_i}{\Delta t} r_{\text{Leray}}(\mathbf{u}^{n+1-i}, \mathbf{g}^{n+1-i}, q). \end{aligned} \quad (22)$$

By choosing the central flux and integrating the forcing term, the convective operator and the Leray projection term by parts once, the consistent boundary condition given in Eq. (12) reduces to contributions from only the acceleration term and the viscous term. All remaining terms cancel on the boundary, as shown in the following. The forcing term is written as

$$r_f(\mathbf{f}, q) := (\mathbf{f}, \nabla q)_{\Omega_e} - (\mathbf{f} \cdot \mathbf{n}, q)_{\partial \Omega_e \setminus \Gamma_h} - (\mathbf{f} \cdot \mathbf{n}, q)_{\partial \Omega_e \cap \Gamma_N}. \quad (23)$$

On the Dirichlet boundary the forcing term  $-(\mathbf{f} \cdot \mathbf{n}, q)_{\partial\Omega_e \cap \Gamma_D}$  cancels with the contribution of the forcing term  $(\mathbf{f} \cdot \mathbf{n}, q)_{\partial\Omega_e \cap \Gamma_D}$  in the consistent boundary condition.

The convective term is formulated in convective formulation and is integrated by parts once. On the Dirichlet boundary, the contribution from the average operator is  $(\mathbf{g} \cdot \nabla) \mathbf{u}$  and the convective contribution from Eq. (12) is  $-(\mathbf{g} \cdot \nabla) \mathbf{u}$ , canceling each other, leading to

$$\begin{aligned} r_{\text{conv}}(\mathbf{u}, \mathbf{g}, q) := & -((\mathbf{u} \cdot \nabla) \mathbf{u}, \nabla q)_{\Omega_e} + (q, \{(\mathbf{u} \cdot \nabla) \mathbf{u}\} \cdot \mathbf{n})_{\partial\Omega_e \setminus \Gamma_h} \\ & + (q, (\mathbf{u} \cdot \nabla) \mathbf{u} \cdot \mathbf{n})_{\partial\Omega_e \cap \Gamma_N}. \end{aligned} \quad (24)$$

The divergence operator for the Leray projection terms yields with boundary conditions

$$r_{\text{Leray}}(\mathbf{u}, \mathbf{g}, q) := -(\nabla q, \mathbf{u})_{\Omega_e} + (q, \{\mathbf{u}\} \cdot \mathbf{n})_{\partial\Omega_e \setminus \Gamma_h} + (q, \mathbf{u} \cdot \mathbf{n})_{\partial\Omega_e \cap \Gamma_N}. \quad (25)$$

The inhomogeneous part of the SIPG formulation includes the remaining parts of the consistent boundary condition (Eq. (12)) and is given by

$$\begin{aligned} r_{\text{SIPG}}(g_p^{n+1}, \mathbf{u}^{n+1-i}, \mathbf{g}^{n+1}, q) := & (q, 2\tau g_p)_{\partial\Omega_e \cap \Gamma_N} - (\nabla q, g_p \mathbf{n})_{\partial\Omega_e \cap \Gamma_N} \\ & - \left( q, \frac{\gamma_0}{\Delta t} \mathbf{g}^{n+1} \cdot \mathbf{n} \right)_{\partial\Omega_e \cap \Gamma_D} \\ & - (q, \nu \nabla \times (\nabla \times \mathbf{u})) \cdot \mathbf{n})_{\partial\Omega_e \cap \Gamma_D}. \end{aligned} \quad (26)$$

Note that the second part of the time derivative involving  $\sum_i^J \alpha_i / \Delta t \mathbf{g}^{n+1-i}$  cancels with the contribution of the Leray projection on the Dirichlet boundary. In the DG setting, the curl-curl term expressing the viscous contribution on the boundary cannot be reformulated into an expression with first derivatives only as provided in [6, 20, 26] for continuous elements. Therefore, employing equal-order interpolation may lead to a loss of accuracy for highly viscous problems when adopting low polynomial degrees. Instead, our approach following Krank et al. [52] is to first compute the vorticity  $\boldsymbol{\omega} := \nabla \times \mathbf{u}$  by standard element-wise  $L^2$  projection to obtain the vorticity, of which we then compute the curl once again to obtain the required  $\nabla \times \boldsymbol{\omega} \equiv \nabla \times \nabla \times \mathbf{u}$ .

## 4.2 Momentum Step

The momentum step consists of finding  $\mathbf{u}^{n+1} \in \mathcal{V}_h^u$  such that

$$l_u(\mathbf{u}^{n+1}, \mathbf{u}^*, \mathbf{g}^{n+1}, \mathbf{v}) = r_u(\mathbf{u}_{i=1, \dots, J}^{n+1-i}, \mathbf{u}^*, \hat{p}^{n+1}, \mathbf{g}^{n+1}, g_p^{n+1}, h_u^{n+1}, \mathbf{v}) \quad (27)$$

holds for all  $\mathbf{v} \in \mathcal{V}_h^u$  and all elements  $\Omega_e \in \Omega_h$ .

The left-hand side  $l_u(\mathbf{u}^{n+1}, \mathbf{u}^*, \mathbf{v})$  consists of the time derivative term  $m(\mathbf{u}, \mathbf{v})$ , the convective term  $c(\mathbf{u}, \mathbf{u}^*, \mathbf{v})$ , and the viscous part  $v(\mathbf{u}, \mathbf{v})$ . For stabilization, a divergence penalty term  $a_{\text{div}}(\mathbf{u}, \mathbf{u}^*, \mathbf{v})$  and a penalty term  $a_{\text{cont}}(\mathbf{u}, \mathbf{u}^*, \mathbf{g}, \mathbf{v})$  enforcing normal continuity [36] are considered, leading to

$$\begin{aligned} l_u(\mathbf{u}^{n+1}, \mathbf{u}^*, \mathbf{g}^{n+1}, \mathbf{v}) := & m(\mathbf{u}^{n+1}, \mathbf{v}) + c(\mathbf{u}^{n+1}, \mathbf{u}^*, \mathbf{v}) + v(\mathbf{u}^{n+1}, \mathbf{v}) \\ & + a_{\text{div}}(\mathbf{u}^{n+1}, \mathbf{u}^*, \mathbf{v}) + a_{\text{cont}}(\mathbf{u}^{n+1}, \mathbf{u}^*, \mathbf{g}^{n+1}, \mathbf{v}). \end{aligned} \quad (28)$$

The time derivative term on the left hand side is given as

$$m(\mathbf{u}, \mathbf{v}) := \left( \frac{\gamma_0}{\Delta t} \mathbf{u}, \mathbf{v} \right)_{\Omega_e}. \quad (29)$$

The convective term  $c(\mathbf{u}, \mathbf{u}^*, \mathbf{v})$  can either be formulated in the convective form  $c_{\text{conv}}(\mathbf{u}, \mathbf{u}^*, \mathbf{v})$  or the divergence form  $c_{\text{div}}(\mathbf{u}, \mathbf{u}^*, \mathbf{v})$ . The upwind flux is used for the convective formulation of the convective term

$$\begin{aligned} c_{\text{conv}}(\mathbf{u}, \mathbf{u}^*, \mathbf{v}) := & (\mathbf{u}^* \cdot \nabla \mathbf{u}, \mathbf{v})_{\Omega_e} - ((\{\mathbf{u}^*\} \cdot \mathbf{n}) \mathbf{u}, \mathbf{v})_{\partial\Omega_e \setminus \Gamma_h} \\ & + ((\{\mathbf{u}^*\} \cdot \mathbf{n}) \{\mathbf{u}\} + 1/2 \{\{\mathbf{u}^*\} \cdot \mathbf{n}\} \cdot \mathbf{n} [\mathbf{u}], \mathbf{v})_{\partial\Omega_e \setminus \Gamma_h} \\ & + (\mathbf{v}, (|\mathbf{u}^* \cdot \mathbf{n}| - \mathbf{u}^* \cdot \mathbf{n}) \mathbf{u})_{\partial\Omega_e \cap \Gamma_D}. \end{aligned} \quad (30)$$

The local Lax-Friedrichs flux is adopted within the divergence formulation of the convective term

$$\begin{aligned} c_{\text{div}}(\mathbf{u}, \mathbf{u}^*, \mathbf{v}) := & -(\mathbf{u} \otimes \mathbf{u}^*, \nabla \mathbf{v})_{\Omega_e} \\ & + ((\{\mathbf{u} \otimes \mathbf{u}^*\} \cdot \mathbf{n}) + 1/2 \Lambda [\mathbf{u}], \mathbf{v})_{\partial\Omega_e \setminus \Gamma_h} \\ & + (\mathbf{v}, |\mathbf{u}^* \cdot \mathbf{n}| \mathbf{u})_{\partial\Omega_e \cap \Gamma_D} + (\mathbf{v}, (\mathbf{u} \otimes \mathbf{u}^*) \cdot \mathbf{n})_{\partial\Omega_e \cap \Gamma_N}. \end{aligned} \quad (31)$$

with  $\Lambda = \zeta_{\text{LF}} \max(|\mathbf{u}_+^* \cdot \mathbf{n}|, |\mathbf{u}_-^* \cdot \mathbf{n}|)$ , where  $\zeta_{\text{LF}}$  can be set to 0.5 to allow for larger timesteps.

**Remark.** Expressing the convective operator in skew-symmetric form does not yield the same benefits (e.g. in form of energy stability) as in the continuous Galerkin setting. This difference arises from the face contributions that appear in both the convective and divergence formulations, even when choosing the same fluxes.

Similar to the pressure operator, the SIPG method is utilized for the viscous part

$$\begin{aligned} v(\mathbf{u}, \mathbf{v}) := & (\nu \nabla \mathbf{u}, \nabla \mathbf{v})_{\Omega_e} - (\nabla \mathbf{v} \cdot \mathbf{n}, \nu \mathbf{u})_{\partial \Omega_e \cap \Gamma_D} - (\mathbf{v}, \nu \nabla \mathbf{u} \cdot \mathbf{n} - 2\nu \tau \mathbf{u})_{\partial \Omega_e \cap \Gamma_D} \\ & - (\nabla \mathbf{v} \mathbf{n}, 1/2 \nu [\![\mathbf{u}]\!] )_{\partial \Omega_e \setminus \Gamma_h} - (\mathbf{v}, \nu (\{\!\{ \nabla \mathbf{u} \mathbf{n} \}\!\} - \tau [\![\mathbf{u}]\!] ))_{\partial \Omega_e \setminus \Gamma_h}. \end{aligned} \quad (32)$$

The stabilization parameter  $\tau$  for tensor-product finite elements is again chosen according to Hillewaert [51]. The divergence penalty term is defined as

$$a_{\text{div}}(\mathbf{u}, \mathbf{u}^*, \mathbf{v}) := \left( \frac{\zeta_D h_e \|\overline{\mathbf{u}^*}\|}{k_u + 1} \nabla \cdot \mathbf{u}, \nabla \cdot \mathbf{v} \right)_{\Omega_e}, \quad (33)$$

with penalty parameter  $\zeta_D = 1$ ,  $\|\overline{\mathbf{u}^*}\|$  being the element-wise volume averaged extrapolated velocity,  $h_e = V_e^{1/3}$  being the characteristic element length, and with  $V_e$  being the element volume [36]. Note that the velocity divergence penalty is related to grad-div stabilization for continuous elements [53, 54].

The continuity penalty term, applied in normal direction on the inner faces and the Dirichlet boundary following [36, 52], is defined as

$$\begin{aligned} a_{\text{cont}}(\mathbf{u}, \mathbf{u}^*, \mathbf{g}, \mathbf{v}) := & (\mathbf{v} \cdot \mathbf{n}, \zeta_C \|\overline{\mathbf{u}^*}\| (\llbracket \mathbf{u} \rrbracket \cdot \mathbf{n}))_{\partial \Omega_e \setminus \Gamma_h} \\ & + (\mathbf{v} \cdot \mathbf{n}, 2\zeta_C \|\overline{\mathbf{u}^*}\| (\mathbf{u} - \mathbf{g}) \cdot \mathbf{n})_{\partial \Omega_e \cap \Gamma_D}, \end{aligned} \quad (34)$$

with penalty parameter  $\zeta_C = 1$ . As the splitting method comes with consistent boundary conditions, the penalty terms can directly be incorporated in the momentum equation. It is also possible to include the terms in a postprocessing (or projection) step as is done in [55].

**Remark.** The divergence and continuity penalty can be seen to enforce a solution space akin to  $H(\text{div})$  elements, where the former regulates the divergence-freeness of the velocity field and the latter the continuity in normal direction.

The right-hand side consists of the forcing term  $f(\mathbf{f}, \mathbf{v})$ , the time-derivative term  $m_r(\mathbf{u}_{i=1, \dots, J}^{n+1-i}, \mathbf{v})$ , the pressure term  $b_p(p, g_p, \mathbf{v})$ , the convective term  $c_r(\mathbf{u}^*, \mathbf{g}, \mathbf{v})$  and the viscous term  $v_r(\mathbf{g}, \mathbf{h}_u, \mathbf{v})$ , and reads as

$$\begin{aligned} r_u := & f(\mathbf{f}, \mathbf{v}) + m_r(\mathbf{u}_{i=1, \dots, J}^{n+1-i}, \mathbf{v}) + b_p(\hat{p}^{n+1}, g_p^{n+1}, \mathbf{v}) \\ & + c_r(\mathbf{u}^*, \mathbf{g}^{n+1}, \mathbf{v}) + v_r(\mathbf{g}^{n+1}, \mathbf{h}_u^{n+1}, \mathbf{v}) \end{aligned} \quad (35)$$

with

$$f(\mathbf{f}, \mathbf{v}) := (\mathbf{f}^{n+1}, \mathbf{v})_{\Omega_e} \quad (36)$$

and the previous time velocities of the BDF integrator,

$$m_r(\mathbf{u}_{i=1, \dots, J}^{n+1-i}, \mathbf{v}) := \left( \sum_{i=1}^J \frac{\alpha_i}{\Delta t} \mathbf{u}^{n+1-i}, \mathbf{v} \right)_{\Omega_e}. \quad (37)$$

The formulation for the pressure gradient term is obtained by integrating by parts twice

$$b_p(p, g_p, \mathbf{v}) := -(\nabla p, \mathbf{v})_{\Omega_e} + (1/2 \llbracket p \rrbracket \mathbf{n}, \mathbf{v})_{\partial \Omega_e \setminus \Gamma_h} + ((p - g_p) \mathbf{n}, \mathbf{v})_{\partial \Omega_e \cap \Gamma_N}. \quad (38)$$

Despite the pressure gradient term only appearing on the right-hand side of the momentum balance equation, numerical results from Fehn et al. [35] indicate that integration by parts is indeed necessary to achieve the expected convergence rates.

The inhomogeneous contributions of the convective term in convective formulation are expressed as

$$c_{r, \text{conv}}(\mathbf{u}^*, \mathbf{g}, \mathbf{v}) := -(\mathbf{v}, (\mathbf{u}^* \cdot \mathbf{n} - |\mathbf{u}^* \cdot \mathbf{n}|) \mathbf{g})_{\partial \Omega_e \cap \Gamma_D}. \quad (39)$$

For the divergence formulation the right-hand side is

$$c_{r, \text{div}}(\mathbf{u}^*, \mathbf{g}, \mathbf{v}) := (\mathbf{v}, -(\mathbf{g} \otimes \mathbf{u}^*) \cdot \mathbf{n} + |\mathbf{u}^* \cdot \mathbf{n}| \mathbf{g})_{\partial \Omega_e \cap \Gamma_D}. \quad (40)$$

The contributions from the viscous part are due to the SIPG discretization

$$v_r(\mathbf{g}, \mathbf{h}_u, \mathbf{v}) := -(\nabla \mathbf{v} \mathbf{n}, \nu \mathbf{g})_{\partial \Omega_e \cap \Gamma_D} + (\mathbf{v}, 2\nu \tau \mathbf{g})_{\partial \Omega_e \cap \Gamma_D} + (\mathbf{h}_u, \mathbf{v})_{\partial \Omega_e \cap \Gamma_N}. \quad (41)$$

### 4.3 Timestepping Algorithm

This section summarizes the timestepping procedure in Alg. 1. For simplicity of presentation, the startup process is omitted here, which either consists of interpolating a given exact solution at the required time instants, using lower-order BDF schemes with increasing order, or other time integrators of appropriate order until the necessary data  $\mathbf{u}^{n+1-i}$  is gathered.

---

#### Algorithm 1 Splitting solver

---

- 1: **function** ADVANCESPLITTINGSOLVER( $\mathbf{u}_{i=1,\dots,J}^{n+1-i}, \Delta t$ )
  - 2:     **parameter update:** select/update time integration and extrapolation constants
  - 3:     **pressure step:** compute the pressure  $\hat{p}^{n+1}$  via (20), i.e., find  $\hat{p}^{n+1} \in \mathcal{V}_h^p$  such that
 
$$l_p(\hat{p}^{n+1}, q) = r_p(\mathbf{u}_{i=1,\dots,J}^{n+1-i}, \mathbf{f}^{n+1}, \mathbf{g}_{i=1,\dots,J}^{n+1-i}, q) \quad \forall q \in \mathcal{V}_h^p, \forall \Omega_e \in \Omega_h.$$
  - 4:     compute velocity extrapolation  $\mathbf{u}^*$  for linearization
  - 5:     **momentum step:** compute the velocity  $\mathbf{u}^{n+1}$  via (27), that is, find  $\mathbf{u}^{n+1} \in \mathcal{V}_h^u$  such that
 
$$\begin{aligned} l_u(\mathbf{u}^{n+1}, \mathbf{u}^*, \mathbf{g}^{n+1}, \mathbf{v}) \\ = r_u(\mathbf{u}_{i=1,\dots,J}^{n+1-i}, \mathbf{u}^*, \hat{p}^{n+1}, \mathbf{g}^{n+1}, g_p^{n+1}, h_u^{n+1}, \mathbf{v}) \quad \forall \mathbf{v} \in \mathcal{V}_h^u, \forall \Omega_e \in \Omega_h. \end{aligned}$$
  - 6:     **return**  $\mathbf{u}_h^{n+1}, p_h^{n+1}$
- 

#### 4.3.1 Similarity to the Higher-Order Dual Splitting under Periodic Boundary Conditions

The higher-order dual splitting [23] is given by

$$\frac{\gamma_0 \mathbf{u}^* - \sum_{i=0}^{J-1} (\alpha_i \mathbf{u}^{n-i})}{\Delta t} = - \sum_{i=0}^{J-1} \beta_i (\mathbf{u}^{n-i} \cdot \nabla) \mathbf{u}^{n-i} + \mathbf{f}^{n+1}, \quad (42)$$

$$-\Delta p^{n+1} = - \frac{\gamma_0}{\Delta t} \nabla \cdot \mathbf{u}^*, \quad (43)$$

$$\mathbf{u}^{**} = \mathbf{u}^* - \frac{\Delta t}{\gamma_0} \nabla p^{n+1}, \quad (44)$$

$$\frac{\gamma_0}{\Delta t} \mathbf{u}^{n+1} - \nu \Delta \mathbf{u}^{n+1} = \frac{\gamma_0}{\Delta t} \mathbf{u}^{**}. \quad (45)$$

Inserting Eq. (42) into (43) leads to the PPE with Leray correction given by Eq. (18). Further, if Eqs. (44) and (42) are inserted into Eq. (45), it is similar to the momentum Eq. (13). The difference is the treatment of the convective term, which is explicit in the dual splitting scheme and semi-implicit in the consistent splitting method presented here. Note, however, that it could also be considered semi-implicitly, see the variant presented in [56] and related work in [24, 30, 43, 57].

For an explicit treatment of the convective operator within the proposed consistent splitting method, the two schemes differ in the boundary conditions only, see Sec. 6. Under periodic boundary conditions, the two schemes are identical, assuming that only the temporal discretization is considered, i.e., when the problem remains continuous in space. For the proposed  $L^2$ -conforming spatial discretization, the right-hand side term of Eq. (42) can be treated with classical flux boundary conditions, whereas the right-hand side of the PPE incorporates the convective term tested against the gradient of the test function, see Eq. (24).

This equivalence raises doubts about the requirements regarding the choice of function spaces for velocity and pressure in the consistent splitting method presented here. The dual splitting method of Karniadakis et al. [23] is known to be subject to an inf-sup condition, while the consistent splitting scheme (without Leray projection) is reportedly not subject to such a condition [26, 45, 58]. Adopting the Leray projection required to obtain the optimal convergence rates for the present formulation, however, might re-introduce the inf-sup condition in some sense. Hence, the potential accuracy loss using equal-order interpolation for viscous flows due to the curl-curl term is not the only reason for choosing  $k_u = k_p + 1$ .

Finally, we remark that the proposed consistent splitting scheme is also advantageous for  $H^1$ -conforming or  $H(\text{div})$ -conforming discretizations, since it avoids the solution of a mass matrix system for step (42) present in the dual splitting method. A comparison of the present splitting scheme and the dual splitting scheme by Karniadakis et al. [23] is provided in Sec. 5.3.

## 5 Numerical Results

This section examines the numerical properties of the devised method. First, convergence in space and time for an example with known analytical solution is demonstrated in Sec. 5.1, thereafter, the schemes' ability to accurately predict fluid mechanical quantities in practically relevant scenarios is evaluated for classical benchmarks being the two-dimensional flow around a cylinder [40] and the Taylor–Green vortex [41] in its three-dimensional setup according to Wang et al. [42]. Matrix-based and matrix-free implementations are publicly available via the `BDFConsistentSplitting` scheme in `ExaDG` [59],<sup>1</sup>

which is based on `deal.II` [60]. The PPE is solved using a conjugate-gradient solver preconditioned by multigrid algorithms, while the momentum equation is solved with a GMRES solver using an inverse mass preconditioner, as the resulting linear system is not symmetric. If not specified otherwise, the relative solver tolerance is set to  $10^{-6}$  and the absolute solver tolerance to  $10^{-12}$ .

### 5.1 Manufactured Solution

First, we focus on the two dimensional Taylor–Green vortex test case [41], see also Hesthaven and Warburton [34]. The solution of the incompressible Navier–Stokes problem is given by

$$\begin{aligned} \mathbf{u}(\mathbf{x}, t) &= \begin{pmatrix} -\sin(2\pi x_2) \\ \sin(2\pi x_1) \end{pmatrix} \exp(-4\nu\pi^2 t) \\ p(\mathbf{x}, t) &= -\cos(2\pi x_1) \cos(2\pi x_2) \exp(-8\nu\pi^2 t) \end{aligned} \quad (46)$$

with the right-hand side being zero,  $\mathbf{f} = \mathbf{0}$ . The domain  $\Omega := [-0.5, 0.5]^2$ , a square of length 1, is considered and the simulation is performed over the time interval  $0 \leq t \leq T = 1$  with the viscosity  $\nu = 0.025$ . The Dirichlet and Neumann boundary conditions and initial conditions are derived from the exact solution. The relative  $L^2$  errors of the velocity and the pressure are computed as

$$\epsilon_p = \left( \frac{\|p - p_h\|_{L^2(\Omega)}}{\|p\|_{L^2(\Omega)}} \right) \Big|_{t=T} \quad \text{and} \quad \epsilon_u = \left( \frac{\|\mathbf{u} - \mathbf{u}_h\|_{L^2(\Omega)}}{\|\mathbf{u}\|_{L^2(\Omega)}} \right) \Big|_{t=T} \quad (47)$$

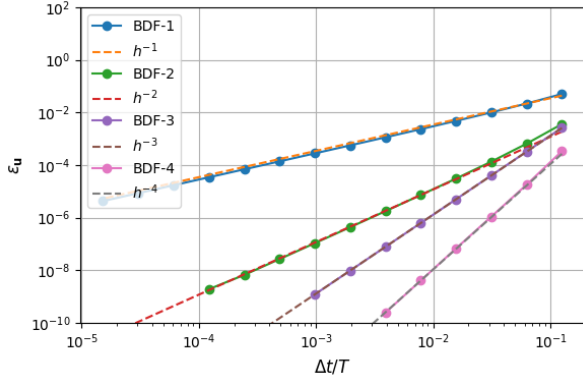
#### 5.1.1 Convergence in Time

To verify the expected convergence rates in time, the grid is uniformly refined four times, yielding a uniform Cartesian grid with  $h_e = 1/32$ . Quadrilateral elements with polynomial degree  $k_u = 5$  for the velocity and  $k_p = 4$  for the pressure are used. Therefore, the error in the spatial discretization is small compared to the error in time. For BDF-1 and BDF-2  $J_c$  and  $J_p$  are chosen equal to  $J$ , while for the other cases,  $J_p = J_c = J - 1$  is used. Fig. 1 shows optimal convergence for BDF-1 to BDF-4, that is,  $\mathcal{O}(\Delta t^J)$ , for both the velocity and the pressure *even though*  $J_c = J - 1$  for  $J > 2$ . In the present scenario, one reaches the level of the spatial error, without observable evidence of a reduction in the convergence rate for  $J > 2$ . However, a reduction to an order of  $J_c = J - 1$  cannot be excluded in general. A thorough analysis of this potential behavior falls outside the scope of the current study.

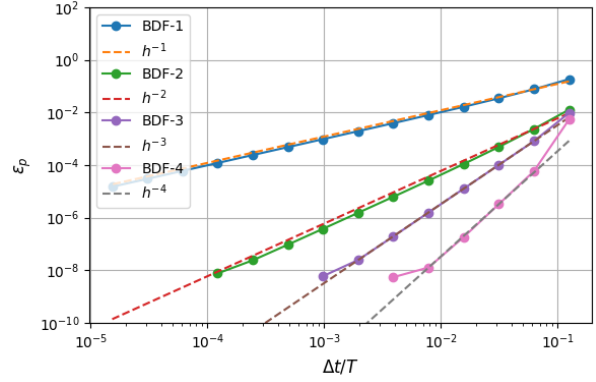
#### 5.1.2 Convergence in Space

To compute the spatial error, the time step size is set to  $6.1035 \times 10^{-5}$  applying the BDF-2 scheme, such that the temporal error is lower than the spatial one. The relative  $L^2$  error under mesh refinement is depicted in Fig. 2. Optimal convergence rates of  $h^{k+1}$  can be observed for all polynomial degrees  $k_u = 2, \dots, 5$  and  $k_p = 1, \dots, 4$  for the velocity and the pressure, respectively. For  $k_u = 2$  the absolute tolerance of the linear solvers is set to  $10^{-8}$  to achieve proper convergence rates for the two finest grids.

<sup>1</sup><https://github.com/exadg/exadg>, retrieved on November 30, 2025.

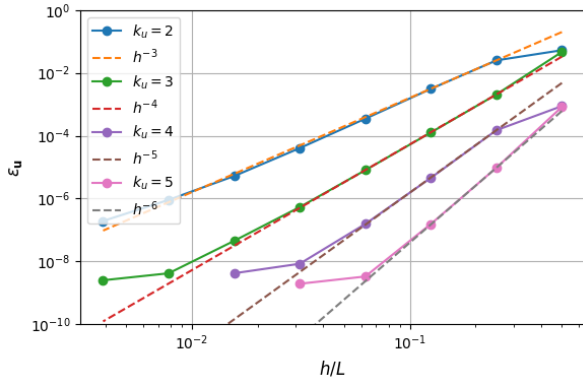


(a) Convergence of the velocity

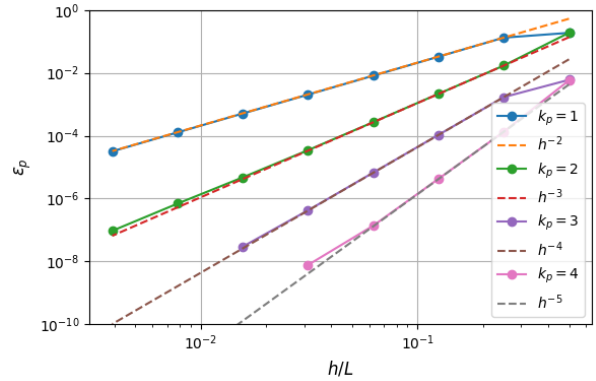


(b) Convergence of the pressure

Figure 1: Temporal convergence of velocity (left) and pressure (right) in the Taylor–Green vortex benchmark as obtained via the consistent splitting scheme for BDF-1 to BDF-4.



(a) Convergence of the velocity



(b) Convergence of the pressure

Figure 2: Spatial convergence of the consistent splitting scheme with different polynomial degrees.

**Remark.** Adding the divergence and continuity penalty terms does not alter the order of convergence, nor effects the magnitude of the error in this specific example. However, disregarding the Leray projection—which in the present form of the splitting scheme merely leads to a modified pressure variable—decreases the convergence order of the method: instead of the optimal convergence rate of  $h^{k_p+1}$ , only  $h^{k_p}$  is observed for the pressure, while the velocity shows rates of  $h^{k_u-1}$  without the Leray projection instead of the optimal  $h^{k_u+1}$ . Similarly, the convergence order in time without Leray projection is impacted. This leads to the conclusion that the addition of the Leray projection is vital for the performance of the presented scheme. Implementation effort and operator complexity are minimal because no additional linear system needs to be solved during the time step.

## 5.2 Flow Around a Cylinder

The flow around a cylinder benchmark, specifically the 2D-3 case proposed by Schäfer et al. [40], is investigated with the aim to demonstrate the effect of employing higher-order polynomial degrees in a practically relevant setting. The geometry considered is a channel with length  $L = 2.2$  and height  $H = 0.41$ . A cylinder centered at  $(0.2, 0.2)$  with a diameter of  $D = 0.1$  is placed in the channel, see Fig. 3. The inflow boundary condition at  $x_1 = 0$  is given as

$$\mathbf{g}_u(x_1 = 0, x_2, t) = \begin{pmatrix} 4U_m \frac{x_2(H-x_2)}{H^2} \sin(\pi t/T) \\ 0 \end{pmatrix}. \quad (48)$$

The average velocity is given as  $U_m = 1.5$  and the viscosity as  $\nu = 10^{-3}$  such that the resulting maximal Reynolds number is  $Re_{max} = 100$ . The time interval is chosen as  $0 \leq t \leq T = 8$ . At  $x_1 = L$ , an open

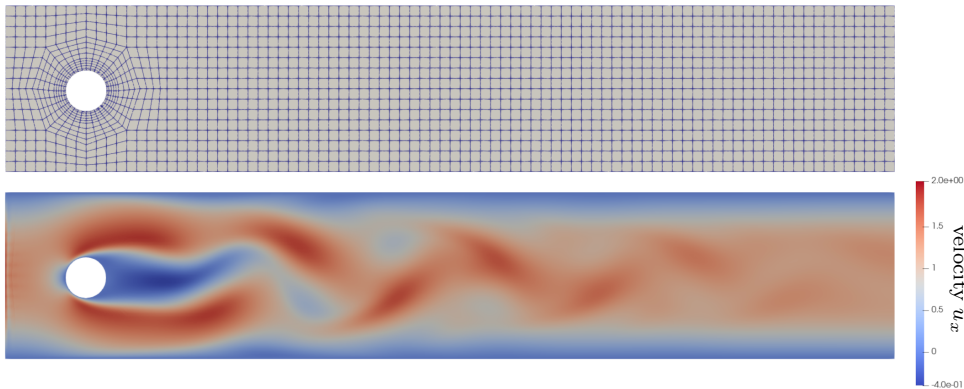


Figure 3: Flow around a cylinder benchmark: computational grid after 2 uniform refinements (top) and horizontal component  $u_x$  of the velocity vector with developed vortex shedding (bottom).

traction (outflow) boundary is given with  $g_p = 0$ , while at all other boundaries the no-slip condition,  $\mathbf{u} = \mathbf{0}$ , is prescribed.

### 5.2.1 Comparison to reference values

The results obtained via the splitting scheme using different polynomial degrees are compared with values from the literature [35, 40, 61]. The results in [35] are obtained with  $k_u = 10$  with around  $10^6$  DoFs. Tab. 1 lists the reported reference values for the maximum lift and drag values and the pressure difference across the cylinder at time  $t = T$ . Tab. 2 lists the values computed with the present method under two refinements (a total of 800 elements, similar to [35]) at different polynomial degrees, using a BDF-3 scheme with a timestep of  $10^{-5}$ . The results show excellent agreement of all quantities for all velocity degrees considered with the literature results.

Table 1: Reference values for the maximum drag and lift values,  $c_{D,\max}$  and  $c_{L,\max}$ , and the pressure difference  $\Delta p$  at  $t = T$  from literature for the 2D-3 test case of the flow around a cylinder benchmark [40].

Reference	$c_{D,\max}$	$c_{L,\max}$	$\Delta p(t = T)$
Schäfer et al. [40] (1996)	$2.95 \pm 2 \cdot 10^{-2}$	$0.48 \pm 1 \cdot 10^{-2}$	$-0.11 \pm 5 \cdot 10^{-3}$
John [61] (2004)	$2.950921575 \pm 5 \cdot 10^{-7}$	$0.47795 \pm 1 \cdot 10^{-4}$	$-0.1116 \pm 1 \cdot 10^{-4}$
Fehn et al. [35] (2017)	2.95091839	0.47788776	-0.11161590

Table 2: Maximum drag and lift values  $c_{D,\max}$  and  $c_{L,\max}$  as obtained with the present scheme for test case 2D-3 using velocity degrees  $k_u = 3, 4, 5$  showing excellent agreement with the reference values given in Tab. 1.

Degree $k_u$	$c_{D,\max}$	$c_{L,\max}$	$\Delta p(t = T)$
3	2.95096212	0.4778764498	-0.11163197467
4	2.95092039	0.4778875586	-0.11161954441
5	2.95091848	0.4778877448	-0.11161596715

### 5.2.2 Higher order time integrators and temporal stability

To showcase the potential of higher-order time integration with the consistent splitting scheme, we demonstrate temporal stability properties for the various linearization variants of the convective term. Tab. 3 considers the explicit, semi-implicit and fully implicit versions of the consistent splitting scheme under increasing target CFL numbers controlling the time step size. For the consistent splitting scheme, the convective formulation of the convective term is chosen, as it permits larger time-step sizes than the divergence formulation in this example. Presented is the maximum drag coefficient obtained with  $k_u = 5$  in a mesh with 800 elements. This spatial discretization is unchanged when increasing the target CFL

number. The explicit method remains stable only for small CFL numbers, whereas the semi-implicit formulation remains robust for CFL numbers up to at least 16. Surprisingly, the fully implicit method does not reach the same CFL limit as the semi-implicit scheme. However, for large CFL values the implicit version yields results that are closer to the reference solution, albeit at the expense of solving a nonlinear system.

Table 3: Maximum drag values  $c_{D,\max}$  (reference value 2.95091839 from [35], see Tab. 1) for test case 2D-3 using the explicit, semi-implicit and implicit versions of the consistent-splitting method under different CFL numbers with BDF-2. Simulations that fail to converge are marked by a dash.

CFL number	0.4	1.0	2.0	4.0	8.0	16.0
Explicit	2.95091536	2.95091496	–	–	–	–
Semi-Implicit	2.95091557	2.95091625	2.95092445	2.95096155	2.95113375	2.95232103
Implicit	2.95091523	2.95091335	2.95091206	2.95091085	2.95091590	–

Now, comparing to the dual splitting scheme, Tab. 4 presents results obtained for the consistent splitting scheme and the dual splitting scheme in their semi-implicit formulation for different BDF schemes under increasing CFL numbers. For the dual-splitting scheme, the continuity and the divergence penalty terms are added in a postprocessing step (see [55]). For better comparison, the same is done in case of the consistent-splitting scheme. Both schemes remain unconditionally stable employing BDF schemes up to and including order 2 (i.e. choosing  $J = J_c = J_p = 2$ ), whereas differences arise for BDF-3 and higher. For the consistent splitting scheme, the extrapolation order of the convective term on the right-hand side of the PPE is set to  $J_c = J - 1$ , which permits larger CFL numbers than the dual splitting scheme, where this term is extrapolated with order  $J_c = J$ . Note that in this case both schemes use  $J_p = J - 1$ . Moreover, the increased accuracy of BDF-3 relative to BDF-2 becomes evident once  $\text{CFL} > 1.0$ .

Table 4: Maximum drag values  $c_{D,\max}$  (reference value 2.95091839 from [35], see Tab. 1) obtained for test case 2D-3 using the semi-implicit consistent splitting (CS) and dual splitting (DS) schemes with different BDF time integration schemes. Simulations that fail to converge are marked by a dash.

CFL number		0.4	1.0	2.0	4.0	8.0	16.0
CS	BDF-2	2.95091557	2.95091625	2.95092445	2.95096155	2.95113375	2.95232103
	BDF-3	2.95091538	2.95091365	2.95092369	2.95092490	2.95093743	2.95106423
	BDF-4	2.95092587	2.95092424	–	–	–	–
DS	BDF-2	2.95092625	2.95092711	2.95093520	2.95097113	2.95113559	2.95222858
	BDF-3	2.95092583	2.95092423	–	–	–	–
	BDF-4	2.95092587	–	–	–	–	–

### 5.3 3D Taylor–Green Vortex

To investigate the performance of the consistent splitting scheme for turbulent flows, we analyze the 3D Taylor–Green vortex problem [41] in the definition proposed by Wang et al. [42], representing transition from a smooth initial condition into turbulence. We consider the spatial domain being a cube with edge length  $2\pi$  centered at the origin, i.e.,  $\Omega_h = [-\pi, \pi]^3$ . The initial condition is given by

$$\begin{aligned}
u_1(\mathbf{x}, t = 0) &= \sin(x_1) \cos(x_2) \cos(x_3) \\
u_2(\mathbf{x}, t = 0) &= -\cos(x_1) \sin(x_2) \cos(x_3) \\
u_3(\mathbf{x}, t = 0) &= 0 \\
p(\mathbf{x}, t = 0) &= \frac{1}{16} (\cos(2x_1) + \cos(2x_2)) (\cos(2x_3) + 2)
\end{aligned} \tag{49}$$

with  $0 \leq t \leq T = 20$  with time step selection aiming for  $\text{CFL} = 0.4$ . The viscosity is chosen such that the Reynolds number is  $\text{Re} = 1/\nu = 1600$ . Periodic boundary conditions are applied to the boundary.

The quantities of interest are the total kinetic energy  $E$  and the molecular energy dissipation rate  $\epsilon$

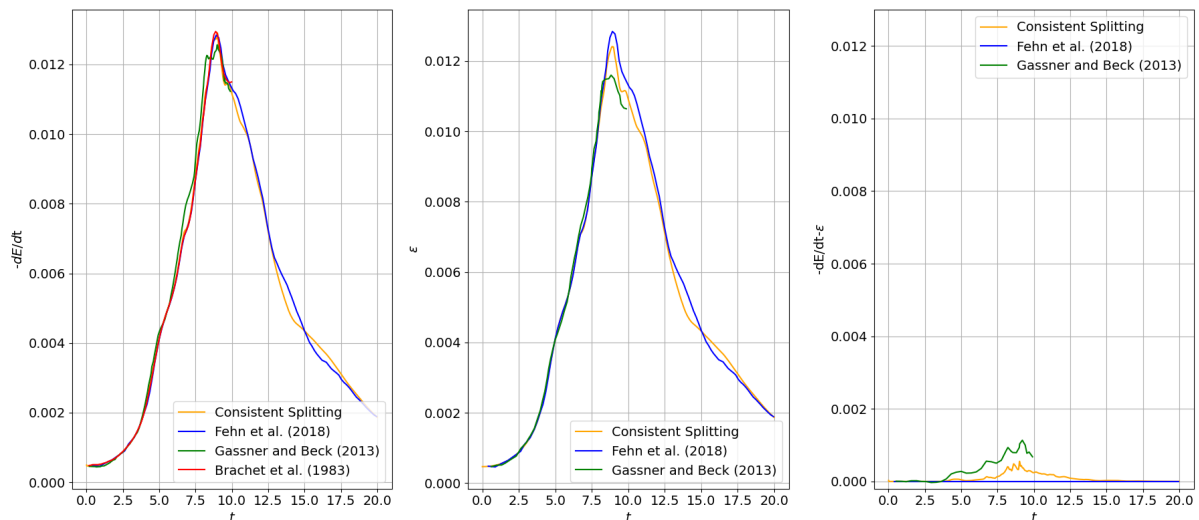
defined as (see, e.g., [36, 62])

$$E := \frac{\int_{\Omega} 1/2 \mathbf{u} \cdot \mathbf{u} \, d\mathbf{x}}{\int_{\Omega} 1 \, d\mathbf{x}}, \quad \epsilon := \frac{\nu \int_{\Omega} \nabla \mathbf{u} : \nabla \mathbf{u} \, d\mathbf{x}}{\int_{\Omega} 1 \, d\mathbf{x}} \quad (50)$$

and the numerical dissipation of the discrete scheme obtained as  $-\frac{dE}{dt} - \epsilon$ .

### 5.3.1 Comparison to reference values

Comparing the consistent splitting scheme to reference values [36, 62, 63] in Fig. 4, one observes that the present scheme indeed yields accurate results. Here, it should be noted that the values in Fehn et al. [36] are obtained via a discretization with 3.22 billion DoFs for the velocity unknowns (refinement level 8 leading to  $256^3$  cells and a polynomial degree of 3) while the results using the presented splitting method were obtained using 21 million velocity DoFs (refinement level 5 yielding  $32^3$  cells and a polynomial degree of 5, giving an effective resolution of  $192^3$  spatial points). Brachet et al. [63] obtained their results by direct numerical simulation and Gassner and Beck [62] utilized implicit large eddy simulation.



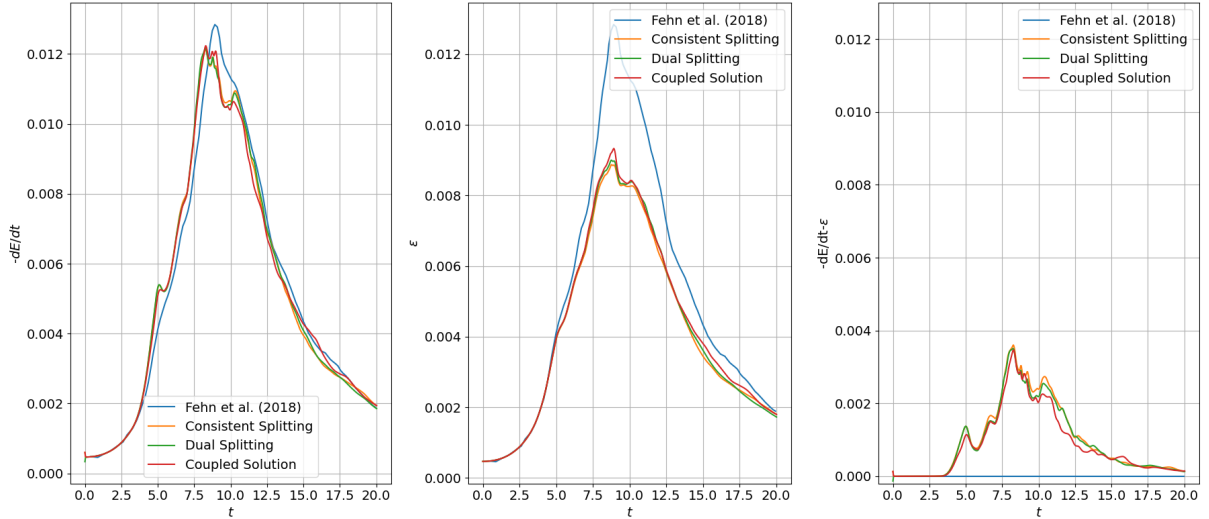
(a) Kinetic energy dissipation rate (b) Molecular energy dissipation rate (c) Numerical dissipation rate

Figure 4: Kinetic energy, molecular dissipation and numerical dissipation of the consistent splitting method with 21 million velocity DoFs in comparison to literature results taken from [36, 62, 63]. Values from [62] are only available for  $t \in [0, 10]$ . Lower numerical dissipation means more accurate, limited by the fixed spatiotemporal resolution chosen.

For a direct comparison of splitting, projection and coupled timestepping algorithms, Fig. 5 shows a comparison with identical spatial resolution with velocity degree  $k_u = 7$  yielding a total of 786,432 velocity DoFs and using different timestepping algorithms:

- i) **dual splitting scheme**: fully explicit, CFL=0.4, convective term in convective formulation [35],
- ii) **coupled solution approach**: fully implicit, CFL=0.4, convective term in convective formulation (see, e.g., [30, 35] among others),
- iii) **consistent splitting scheme**: semi-implicit, CFL=0.4, convective term in convective formulation (this work).

Results demonstrate that all these methods yield comparable results, only showing minor differences between the schemes using *the same spatial resolution*. For reference, the reference results from Fehn et al. [36] are included once again in Fig. 5. All three schemes, i.e., the dual splitting scheme, the coupled solution approach as well as the splitting scheme are implemented in ExaDG [55, 59].



(a) Kinetic energy dissipation rate (b) Molecular energy dissipation rate (c) Numerical dissipation rate

Figure 5: Comparison between the solutions of the coupled solution approach, the dual splitting scheme and the consistent splitting with 786432 velocity DoFs. All schemes yield similar results and compare well against the reference solution from Fehn et al. [36], which uses the dual splitting scheme with 3.221 billion DoFs. Lower numerical dissipation means more accurate, limited by the fixed spatiotemporal resolution chosen.

### 5.3.2 Higher order time integrators and temporal stability

In order to show the effect of higher-order time integrators on the numerical dissipation, we fix the spatial discretization and target CFL number to 1.6 (stability limit for BDF-4) and increase the time integration order using the semi-implicit variant of the consistent splitting scheme. Again we choose  $J_c = J_p = J$  for BDF-1 and BDF-2, while for BDF-3 and BDF-4 they are selected as  $J_c = J_p = J - 1$ . The results presented in Fig. 6 highlight that the BDF-1 scheme exhibits higher numerical dissipation compared to the other schemes. The BDF-2 scheme is close to the higher order schemes but still shows deviations in the dissipation rate  $\epsilon$ . The BDF-3 and BDF-4 schemes differ for  $t > 14.0$  in the dissipation rate  $\epsilon$ , otherwise their results are rather similar, indicating that the spatial error is dominant. The increased numerical dissipation seen in the initial time steps stems for BDF-2 and higher stem from the initialization procedure, which includes single time steps of lower-order methods until the required BDF startup data is gathered.

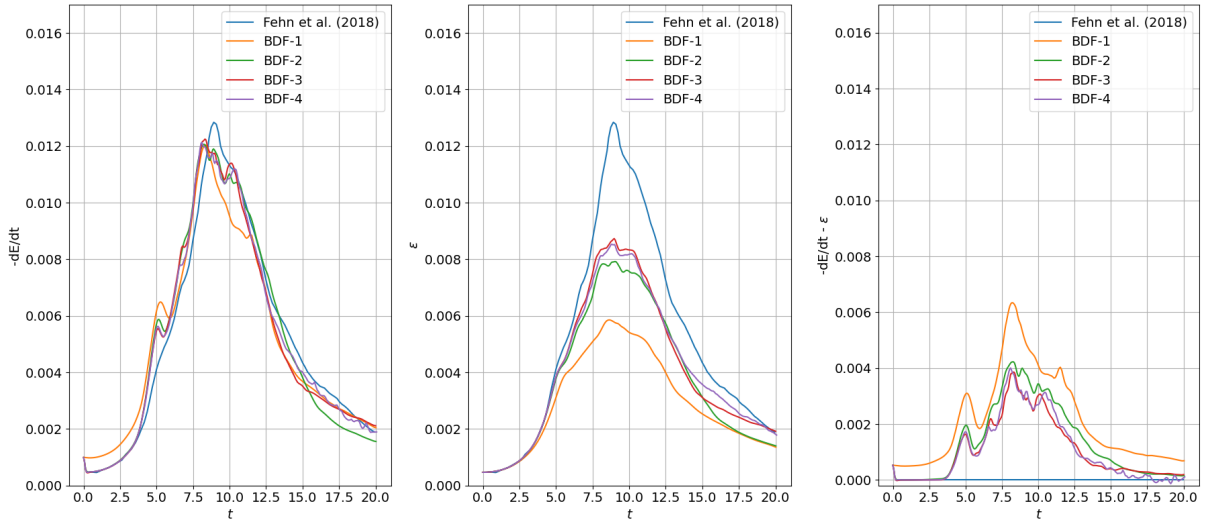
Finally, to compare the schemes under varying CFL numbers using the **semi-implicit** linearization variants, we define the total numerically dissipated energy as

$$\int_{t=0}^{t=20} -\frac{dE}{dt} - \epsilon dt = -(E(t=20) - E(t=0)) - \int_{t=0}^{t=20} \epsilon dt. \quad (51)$$

To assess the influence of the extrapolation order  $J_c$  of the convective term, we compare the consistent splitting method for the cases  $J_c = J - 1$  and  $J_c = J$ . For completeness, results obtained with the dual splitting scheme are also included. As BDF-1 is too dissipative and BDF-4 yields results comparable to those of BDF-3, Tab. 5 shows the total numerically dissipated energy for BDF-2 and BDF-3. Again, the penalty terms are applied to all schemes in a postprocessing step. With the choice  $J_c = J_p = J - 1$ , the consistent splitting method using BDF-3 remains stable at higher CFL numbers compared to the consistent splitting method and the dual splitting scheme with  $J_c = J$  and  $J_p = J - 1$ , while producing results of similar quality.

The results indicate that selecting  $J_c = J - 1$  rather than  $J_c = J$  in the consistent splitting method increases robustness without compromising accuracy. A comparison between BDF-2 and BDF-3 again demonstrates the improved accuracy of the higher-order method.

In summary, the results in this section indicate that i) the scheme is higher-order accurate in space and time, ii) implicit and semi-implicit linearization variants allow target CFL numbers (much) larger



(a) Kinetic energy dissipation rate (b) Molecular energy dissipation rate (c) Numerical dissipation rate

Figure 6: Kinetic energy, molecular dissipation and numerical dissipation of the consistent splitting method with different BDF schemes at a CFL number of 1.6. Lower numerical dissipation means more accurate, limited by the fixed spatiotemporal resolution chosen.

Table 5: Total numerically dissipated energy obtained via the semi-implicit consistent splitting (CS, when used with  $J_c = J - 1$ , and CS\*, when used with  $J_c = J$ ) and dual splitting (DS) schemes with different BDF time integration schemes. Lower numerical dissipation means more accurate, limited by the fixed spatiotemporal resolution chosen. Simulations that fail to converge are marked by a dash.

CFL number		0.4	1.0	2.0	4.0
CS	BDF-2	0.02051	0.02351	0.02873	0.03466
	BDF-3	0.01983	0.02152	0.01933	0.01255
CS*	BDF-3	0.01985	0.02179	-	-
DS	BDF-2	0.02043	0.02342	0.02846	0.03461
	BDF-3	0.01982	0.02174	-	-

than 1 in practical examples, iii) BDF-3 and higher can be used to improve accuracy when using larger time steps also for non-smooth solutions showcased in the 3D Taylor–Green vortex benchmark, iv) the consistent splitting scheme with  $J_c = J_p = J - 1$  shows improved stability for BDF-3 compared to the dual splitting scheme and similar accuracy to the coupled solution approach.

## 6 Concluding Remarks

This work proposes a discontinuous Galerkin spatial discretization of the consistent splitting scheme by Liu [26], with a focus on the formulation of flux terms in an  $L^2$ -conforming setting and the incorporation of consistent boundary conditions. The convective term is formulated in a semi-implicit manner, overcoming the strict CFL condition of an explicit formulation while avoiding the solution of a nonlinear system, which would otherwise result from a fully implicit formulation. By choosing appropriate fluxes for the divergence of the convective operator, the forcing term and the divergence of the velocity for the PPE and integrating each contribution by part once, the consistent pressure boundary condition reduces to contributions from only the acceleration and viscous term. In comparison to Liu et al. [45], the extrapolation order of the term is *lowered* without impacting the temporal convergence rate as shown in section 5.1, but leading to improved stability with higher order BDF schemes as observed also for the related scheme by Karniadakis et al. [23].

For stabilization, a continuity penalty term and a divergence penalty term are added, while Leray projection is used to improve mass conservation. In contrast to a continuous Galerkin discretization, rewriting the curl-curl term using the Gauss theorem (on each element individually for  $L^2$ -conforming

DG adopted herein) and replacing the second-order derivatives with first-order ones similar to [26] or [20] leads to a decrease in the observed convergence rates.

Lowest equal-order discretizations with the present scheme might therefore lead to a loss of accuracy if the curl-curl term cannot be resolved sufficiently for highly viscous problems, since the curl-curl term cannot be represented. Note here that using inf-sup stable pairs, as implicitly required by the Leray projection, being the projection onto a divergence-free space, these drawbacks seem negligible. From a performance perspective, the pressure Poisson equation often constitutes the computational bottleneck, such that a richer velocity approximation as used in an inf-sup stable approach is often preferred.

Despite these minor limitations, the proposed work offers two main advantages: i) compared to the coupled solution approach with a saddle-point linear system, velocity and pressure are decoupled, leading to smaller problems that can be effectively preconditioned by standard tools, and ii) compared to standard projection methods, splitting errors are avoided. The splitting errors often lead to spurious pressure boundary layers, introduced by artificial boundary conditions formulated to render the pressure Poisson problem solvable. Additionally, this renders BDF-3 and BDF-4 possible choices for increased accuracy, albeit with the usual limitations due to the missing A-stability of those time integrators.

The variant considered within this work is demonstrated to yield higher-order convergence rates in space and time in an example with known analytical solution, numerically confirming the formulated claims. Further, we show excellent agreements with state-of-the-art incompressible flow solvers in practically relevant benchmarks being the flow past a cylinder problem and the Taylor–Green vortex problem, see Schäfer et al. [40] and Taylor and Green [41], Wang et al. [42]. In the latter example, the scheme is compared to its closest competitor, the dual splitting scheme by Karniadakis et al. [23], showing very much similar performance, but with the important difference being that i) the present scheme is not affected by splitting errors, and ii) extensions were recently shown to be unconditionally stable in time also for BDF-3 and even higher [27]—a property previously only proven for other splitting or projection schemes *up to second order*, albeit at the price of potentially higher error constants. Consistent splitting schemes are thus great candidates for the numerical solution of incompressible flow problems. In this sense, the present work is a step towards the successful  $L^2$ -conforming discontinuous Galerkin discretization of this family of methods.

To avoid the need for additional stabilization terms, especially the continuity-stabilization, the consistent-splitting scheme can be extended to H(div) conforming elements for the velocity variables, while keeping the  $L^2$  discretizations as the natural ansatz space for the PPE. This leads to questions regarding the performance of these methods taking approximation quality and time to solution into account, where ongoing developments on the preconditioning of the momentum equation in convection-dominated scenarios play a key role.

## Acknowledgements

This work received support by the German Federal Ministry of Research, Technology and Space (BMFTR) through project “PDExa: Optimized Software Methods for Solving Partial Differential Equations on Exascale Supercomputers”, grant agreement nos. 16ME0637K, 16ME0638, and 16ME0640 and the European Union – NextGenerationEU, the EuroHPC joint undertaking Centre of Excellence dealii-X, grant agreement no. 101172493, by the German research foundation through project no. 524455704 (“High-Performance Simulation Tools for Hemodynamics”), and by BREATHE, an ERC-2020-ADG Project, Grant Agreement ID 101021526. The authors thank W.A. Wall and M. Bergbauer for the inspiring discussions and their support.

## Appendix

Starting from the dual splitting in time discrete formulation Eqs. (42) - (45):

$$\begin{aligned}\frac{\gamma_0 \mathbf{u}^* - \sum_{i=0}^{J-1} (\alpha_i \mathbf{u}^{n-i})}{\Delta t} &= - \sum_{i=0}^{J-1} \beta_i (\mathbf{u}^{n-i} \cdot \nabla) \mathbf{u}^{n-i} + \mathbf{f}^{n+1} \\ -\Delta p^{n+1} &= - \frac{\gamma_0}{\Delta t} \nabla \cdot \mathbf{u}^* \\ \mathbf{u}^{**} &= \mathbf{u}^* - \frac{\Delta t}{\gamma_0} \nabla p^{n+1} \\ \frac{\gamma_0}{\Delta t} \mathbf{u}^{n+1} - \nu \Delta \mathbf{u}^{n+1} &= \frac{\gamma_0}{\Delta t} \mathbf{u}^{**}\end{aligned}$$

Rewriting the explicit convection step gives

$$\frac{\gamma_0}{\Delta t} \mathbf{u}^* = - \sum_{i=0}^{J-1} \beta_i (\mathbf{u}^{n-i} \cdot \nabla) \mathbf{u}^{n-i} + \mathbf{f}^{n+1} + \sum_{i=0}^{J-1} \frac{\alpha_i}{\Delta t} \mathbf{u}^{n-i}$$

Inserting into the Poisson Eq. (43) leads to

$$-\Delta p^{n+1} = - \frac{\gamma_0}{\Delta t} \nabla \cdot \mathbf{u}^* = \nabla \cdot \left( \sum_{i=0}^{J-1} \beta_i (\mathbf{u}^{n-i} \cdot \nabla) \mathbf{u}^{n-i} - \mathbf{f}^{n+1} - \sum_{i=0}^{J-1} \frac{\alpha_i}{\Delta t} \mathbf{u}^{n-i} \right)$$

which is equal to PPE (18) with Leray projection. Further, the Helmholtz like Eq. (45) can be written by inserting the definitions of  $\mathbf{u}^*$  and  $\mathbf{u}^{**}$  as

$$\begin{aligned}\frac{\gamma_0}{\Delta t} \mathbf{u}^{n+1} - \nu \Delta \mathbf{u}^{n+1} &= \frac{\gamma_0}{\Delta t} \mathbf{u}^{**} = \frac{\gamma_0}{\Delta t} \mathbf{u}^* - \nabla p^{n+1} \\ &= - \sum_{i=0}^{J-1} \beta_i (\mathbf{u}^{n-i} \cdot \nabla) \mathbf{u}^{n-i} + \mathbf{f}^{n+1} + \sum_{i=0}^{J-1} \frac{\alpha_i}{\Delta t} \mathbf{u}^{n-i} - \nabla p^{n+1}\end{aligned}$$

which gives the momentum Eq. (13) with an explicit convection term

$$\frac{\gamma_0}{\Delta t} \mathbf{u}^{n+1} - \nu \Delta \mathbf{u}^{n+1} = \mathbf{f}^{n+1} - \sum_{i=0}^{J-1} \beta_i (\mathbf{u}^{n-i} \cdot \nabla) \mathbf{u}^{n-i} + \sum_{i=0}^{J-1} \frac{\alpha_i}{\Delta t} \mathbf{u}^{n-i} - \nabla p^{n+1}.$$

## References

- [1] D. Boffi, F. Brezzi, and M. Fortin. *Mixed Finite Element Methods and Applications*, volume 44. Springer Berlin Heidelberg, Berlin, Heidelberg, 2013.
- [2] V. John. *Finite Element Methods for Incompressible Flow Problems*. Springer International Publishing, Basel, 2016.
- [3] P. Hood and C. Taylor. Navier-Stokes equations using mixed interpolation. In J.T. Oden, O.C. Zienkiewicz, R.H. Gallagher, and C. Taylor, editors, *Finite Element Methods in Flow Problems*, pages 57–66, Huntsville, 1974. UAH Press.
- [4] F. Brezzi and J. Pitkäranta. On the stabilization of finite element approximations of the Stokes equations. In W. Hackbusch, editor, *Efficient Solutions of Elliptic Systems. Notes on Numerical Fluid Mechanics*, volume 10, pages 11–19, Wiesbaden, 1984.
- [5] T.J.R. Hughes, L.P. Franca, and M. Balestra. A new finite element formulation for computational fluid dynamics: V. Circumventing the Babuška-Brezzi condition: A stable Petrov-Galerkin formulation of the Stokes problem accommodating equal-order interpolations. *Comput. Methods Appl. Mech. Eng.*, 59(1):85–99, 1986.

- [6] D.R.Q. Pacheco, R. Schussnig, O. Steinbach, and T.-P. Fries. A global residual-based stabilization for equal-order finite element approximations of incompressible flows. *Int. J. Numer. Methods Eng.*, 122(8):2075–2094, 2021.
- [7] R. Schussnig, D.R.Q. Pacheco, and T.-P. Fries. Robust stabilised finite element solvers for generalised Newtonian fluid flows. *J. Comput. Phys.*, 442:110436, 2021.
- [8] J. Cahouet and J.-P. Chabard. Some fast 3D finite element solvers for the generalized Stokes problem. *Int. J. Numer. Meth. Fluids*, 8(8):869–895, 1988.
- [9] M. Benzi and M.A. Olshanskii. An augmented Lagrangian-based approach to the Oseen problem. *SIAM J. Sci. Comput.*, 28(6):2095–2113, 2006.
- [10] M. Benzi, M.A. Olshanskii, and Z. Wang. Modified augmented Lagrangian preconditioners for the incompressible Navier-Stokes equations. *Int. J. Numer. Meth. Fluids*, 66(4):486–508, 2011.
- [11] T. Heister and G. Rapin. Efficient augmented Lagrangian-type preconditioning for the Oseen problem using Grad-Div stabilization. *Int. J. Numer. Meth. Fluids*, 71(1):118–134, 2013.
- [12] C. Lohmann and S. Turek. Augmented Lagrangian acceleration of global-in-time pressure Schur complement solvers for incompressible Oseen equations. *J. Math. Fluid Mech.*, 26(2):27, 2024. doi: 10.1007/s00021-024-00862-7.
- [13] Y. Shih, G. Stadler, and F. Wechsung. Robust multigrid techniques for augmented Lagrangian preconditioning of incompressible stokes equations with extreme viscosity variations. *SIAM J. Sci. Comput.*, 45(3):27–53, 2023.
- [14] H.C. Elman, D.J. Silvester, and A.J. Wathen. *Finite Elements and Fast Iterative Solvers: With Applications in Incompressible Fluid Dynamics*. Oxford University Press, Oxford, 2014.
- [15] D. Kay, D. Loghin, and A. Wathen. A preconditioner for the steady-state Navier–Stokes equations. *SIAM J. Sci. Comput.*, 24(1):237–256, 2003.
- [16] H. Elman, V.E. Howle, J. Shadid, D. Silvester, and R. Tuminaro. Least squares preconditioners for stabilized discretizations of the Navier–Stokes equations. *SIAM J. Sci. Comput.*, 30(1):290–311, 2008.
- [17] H.C. Elman and R.S. Tuminaro. Boundary conditions in approximate commutator preconditioners for the Navier-Stokes equations. *Electron. Trans. Numer. Anal.*, 35:257–280, 2009.
- [18] T.C. Clevenger and T. Heister. Comparison between algebraic and matrix-free geometric multigrid for a Stokes problem on adaptive meshes with variable viscosity. *Numer. Linear Algebra Appl.*, 28(5):e2375, 2021.
- [19] M. Kronbichler, A. Diagne, and H. Holmgren. A fast massively parallel two-phase flow solver for microfluidic chip simulation. *Int. J. High Perform. Comput. Appl.*, 32(2):266–287, 2018.
- [20] M. Creff and J.-L. Guermond. Consistent pressure formulation of the Stokes problem and approximation thereof. *Comput. Methods Appl. Mech. Eng.*, 447:118333, 2025.
- [21] L.J.P. Timmermans, P.D. Mineev, and F.N. van de Vosse. An approximate projection scheme for incompressible flow using spectral elements. *Int. J. Numer. Meth. Fluids*, 22(7):673–688, 1996.
- [22] J. Guermond and J. Shen. On the error estimates for the rotational pressure-correction projection methods. *Math. Comput.*, 73:1719–1737, 2003.
- [23] G.E. Karniadakis, M. Israeli, and S.A. Orszag. High-order splitting methods for the incompressible Navier-Stokes equations. *J. Comput. Phys.*, 97(2):414–443, 1991.
- [24] J.L. Guermond and J. Shen. Velocity-correction projection methods for incompressible flows. *SIAM J. Numer. Anal.*, 41(1):112–134, 2003.
- [25] J.L. Guermond and J. Shen. A new class of truly consistent splitting schemes for incompressible flows. *J. Comput. Phys.*, 192(1):262–276, 2003.

- [26] J. Liu. Open and traction boundary conditions for the incompressible Navier–Stokes equations. *J. Comput. Phys.*, 228(19):7250–7267, 2009.
- [27] F. Huang and J. Shen. Stability and error analysis of a new class of higher-order consistent splitting schemes for the navier–stokes equations. *arXiv*, 2025. doi: 10.48550/arXiv.2507.01296.
- [28] J. Deteix and D. Yakoubi. Shear rate projection schemes for non-Newtonian fluids. *Comput. Methods Appl. Mech. Eng.*, 354:620–636, 2019.
- [29] D.R.Q. Pacheco, R. Schussnig, and T.-P. Fries. An efficient split-step framework for non-Newtonian incompressible flow problems with consistent pressure boundary conditions. *Comput. Methods Appl. Mech. Eng.*, 382:113888, 2021.
- [30] R. Schussnig, N. Fehn, D.R.Q. Pacheco, and M. Kronbichler. Higher-order discontinuous Galerkin splitting schemes for fluids with variable viscosity. *Comput. Methods Appl. Mech. Eng.*, 448:118497, 2026.
- [31] D.R.Q. Pacheco and R. Schussnig. Consistent pressure Poisson splitting methods for incompressible multi-phase flows: eliminating numerical boundary layers and inf-sup compatibility restrictions. *Comput. Mech.*, 70:977–992, 2022.
- [32] D.R.Q. Pacheco and R. Schussnig. A fully segregated and unconditionally stable IMEX scheme for dispersed multiphase flows. *ESAIM: M2AN*, 59:2863–2893, 2025.
- [33] R. Schussnig, D.R.Q. Pacheco, and T.-P. Fries. Efficient split-step schemes for fluid–structure interaction involving incompressible generalised Newtonian flows. *Comput. Struct.*, 260:106718, 2022.
- [34] J. Hesthaven and T. Warburton. *Nodal Discontinuous Galerkin Methods: Algorithms, Analysis, and Applications*, volume 54. Springer Nature, 2007.
- [35] N. Fehn, W.A. Wall, and M. Kronbichler. On the stability of projection methods for the incompressible Navier–Stokes equations based on high-order discontinuous Galerkin discretizations. *J. Comput. Phys.*, 351:392–421, 2017.
- [36] N. Fehn, W.A. Wall, and M. Kronbichler. Robust and efficient discontinuous Galerkin methods for under-resolved turbulent incompressible flows. *J. Comput. Phys.*, 372:667–693, 2018.
- [37] H. Johnston and J.-G. Liu. Accurate, stable and efficient navier–stokes solvers based on explicit treatment of the pressure term. *J. Comput. Phys.*, 199(1):221–259, 2004.
- [38] R.R. Rosales, B. Seibold, D. Shirokoff, and D. Zhou. High-order finite element methods for a pressure poisson equation reformulation of the Navier–Stokes equations with electric boundary conditions. *Comput. Methods Appl. Mech. Eng.*, 373:113451, 2021.
- [39] M. Li, Y. Cheng, J. Shen, and X. Zhang. A bound-preserving high order scheme for variable density incompressible Navier-Stokes equations. *J. Comput. Phys.*, 425:109906, 2021.
- [40] M. Schäfer, S. Turek, F. Durst, E. Krause, and R. Rannacher. Benchmark computations of laminar flow around a cylinder. In E.H. Hirschel, editor, *Flow Simulation with High-Performance Computers II: DFG Priority Research Programme Results 1993–1995*, pages 547–566. Vieweg&Teubner Verlag, Wiesbaden, 1996.
- [41] G.I. Taylor and A.E. Green. Mechanism of the production of small eddies from large ones. *Proc. R. Soc. A: Math. Phys. Eng. Sci.*, 158(895):499–521, 1937.
- [42] Z.J. Wang, K. Fidkowski, R. Abgrall, F. Bassi, D. Caraeni, A. Cary, H. Deconinck, R. Hartmann, K. Hillewaert, H.T. Huynh, N. Kroll, G. May, P.-O. Persson, B. van Leer, and M. Visbal. High-order CFD methods: current status and perspective. *Int. J. Numer. Methods Fluids*, 72(8):811–845, 2013.
- [43] J.L. Guermond, P. Mineev, and Jie Shen. An overview of projection methods for incompressible flows. *Comput. Methods Appl. Mech. Eng.*, 195(44-47):6011–6045, 2006.
- [44] R. Schussnig. *Generalised Newtonian Fluids in Cardiovascular Fluid–Structure Interaction*. PhD thesis, Graz University of Technology, 2022.

- [45] J.-G. Liu, J. Liu, and R.L. Pego. Stable and accurate pressure approximation for unsteady incompressible viscous flow. *J. Comput. Phys.*, 229(9):3428–3453, 2010.
- [46] E. Hairer, S.P. Nørsett, and G. Wanner. *Solving Ordinary Differential Equations I - Nonstiff problems*, volume 8 of *Springer Series in Computational Mathematics*. Springer Berlin Heidelberg, Berlin, Heidelberg, 2nd edition, 1993.
- [47] U.M. Ascher, S.J. Ruuth, and B.T.R. Wetton. Implicit-explicit methods for time-dependent partial differential equations. *SIAM J. Numer. Anal.*, 32(3):797–823, 1995.
- [48] D.N. Arnold. An interior penalty finite element method with discontinuous elements. *SIAM J. Numer. Anal.*, 19(4):742–760, 1982.
- [49] D.N. Arnold, F. Brezzi, B. Cockburn, and D. Marini. Discontinuous Galerkin methods for elliptic problems. In B Cockburn, G. Karniadakis, and C.-W. Shu, editors, *Discontinuous Galerkin Methods: Theory, Computation and Applications*, volume 11 of *Springer Lecture Notes in Computational Science and Engineering*, pages 89–101. Springer Berlin Heidelberg, 2000.
- [50] D.N. Arnold, F. Brezzi, B. Cockburn, and D. Marini. Unified analysis of discontinuous Galerkin methods for elliptic problems. *SIAM J. Numer. Anal.*, 39(5):1749–1779, 2002.
- [51] K. Hillewaert. *Development of the discontinuous Galerkin method for high-resolution, large scale CFD and acoustics in industrial geometries*. PhD thesis, Université catholique de Louvain, 2013.
- [52] B. Krank, N. Fehn, W. Wall, and M. Kronbichler. A high-order semi-explicit discontinuous Galerkin solver for 3D incompressible flow with application to DNS and LES of turbulent channel flow. *J. Comput. Phys.*, 348, 07 2016.
- [53] M. Akbas, A. Linke, L.G. Rebholz, and P.W. Schroeder. The analogue of grad–div stabilization in DG methods for incompressible flows: Limiting behavior and extension to tensor-product meshes. *Comput. Methods Appl. Mech. Eng.*, 341:917–938, 2018.
- [54] M. Olshanskii, G. Lube, T. Heister, and J. Löwe. Grad–div stabilization and subgrid pressure models for the incompressible Navier–Stokes equations. *Comput. Methods Appl. Mech. Eng.*, 198(49):3975–3988, 2009.
- [55] N. Fehn. *Robust and Efficient Discontinuous Galerkin Methods for Incompressible Flows*. PhD thesis, Technische Universität München, 2021.
- [56] A.I. Liosi, H. Wüstenberg, P. Khurana, S. Sherwin, J. Hoessler, A. Swift, and A. Chatzopoulos. Comparing efficient implicit time-stepping techniques for highly resolved simulations using industrial geometries. In *AIAA SCITECH 2025 Forum*. American Institute of Aeronautics and Astronautics, 2025.
- [57] S. Sherwin. A substepping Navier–Stokes splitting scheme for spectral/hp element discretisations. In K. Matsuno, A. Ecer, N. Satofuka, J. Periaux, and P. Fox, editors, *Parallel Computational Fluid Dynamics 2002*, pages 43–52. North-Holland, Amsterdam, 2003.
- [58] J. Liu, J. Liu, and R. Pego. Error estimates for finite-element Navier–Stokes solvers without standard inf-sup conditions. *Chin. Annal. Math. Ser. B*, 30:743–768, 11 2009.
- [59] D. Arndt, N. Fehn, G. Kanschat, K. Kormann, M. Kronbichler, P. Munch, W.A. Wall, and J. Witte. ExaDG: High-order discontinuous Galerkin for the exa-scale. In H.-J. Bungartz, S. Reiz, B. Uekermann, P. Neumann, and W. E. Nagel, editors, *Software for exascale computing-SPPEXA 2016-2019*, pages 189–224, Cham, 2020. Springer International Publishing.
- [60] D. Arndt, W. Bangerth, M. Bergbauer, B. Blais, M. Fehling, R. Gassmüller, T. Heister, L. Heltai, M. Kronbichler, M. Maier, P. Munch, S. Scheuerman, B. Turcksin, S. Uzunbajakau, D. Wells, and M. Wichrowski. The deal.ii library, version 9.7. *J. Numer. Math.*, 2025. URL <https://doi.org/10.1515/jnma-2025-0115>.
- [61] V. John. Reference values for drag and lift of a two-dimensional time-dependent flow around a cylinder. *Int. J. Numer. Methods Fluids*, 44(7):777–788, 2004. doi: 10.1002/flid.679.

- [62] G.J. Gassner and A.D. Beck. On the accuracy of high-order discretizations for underresolved turbulence simulations. *Theor. Comput. Fluid Dyn.*, pages 221–237, 2013.
- [63] M.E. Brachet, D.I. Meiron, B.G. Nickel, R.H. Morf, U. Frisch, and S.A. Orszag. Small-scale structure of the Taylor–Green vortex. *J. Fluid Mech.*, 130:411–452, 1983.